Draft version February 1, 2014
Preprint typeset using LaTeX style emulateapj v. 2/16/10

arXiv:1008.5150v1 [astro-ph.EP] 30 Aug 2010

THE DEUTERIUM-BURNING MASS LIMIT FOR BROWN DWARFS AND GIANT PLANETS

David S. Spiegel[1], Adam Burrows[1], John A. Milsom[2]
[1]Department of Astrophysical Sciences, Peyton Hall, Princeton University, Princeton, NJ 08544
[2]Department of Physics, The University of Arizona, Tucson, AZ 85721
Draft version February 1, 2014

ABSTRACT

There is no universally acknowledged criterion to distinguish brown dwarfs from planets. Numerous studies have used or suggested a definition based on an object's mass, taking the ∼13-Jupiter mass (M_J) limit for the ignition of deuterium. Here, we investigate various deuterium-burning masses for a range of models. We find that, while $13M_J$ is generally a reasonable rule of thumb, the deuterium fusion mass depends on the helium abundance, the initial deuterium abundance, the metallicity of the model, and on what fraction of an object's initial deuterium abundance must combust in order for the object to qualify as having burned deuterium. Even though, for most proto-brown dwarf conditions, 50% of the initial deuterium will burn if the object's mass is $\sim(13.0 \pm 0.8)M_J$, the full range of possibilities is significantly broader. For models ranging from zero-metallicity to more than three times solar metallicity, the deuterium burning mass ranges from ∼11.0 M_J (for 3-times solar metallicity, 10% of initial deuterium burned) to ∼16.3 M_J (for zero metallicity, 90% of initial deuterium burned).

Subject headings: radiative transfer – stars: low-mass, brown dwarfs – stars: evolution

1. INTRODUCTION

The year 1995 heralded both the first unambiguous detection of a brown dwarf (Oppenheimer et al. 1995) and the first unambiguous detections of planets beyond our solar system (Mayor & Queloz 1995; Marcy & Butler 1996). Many of the first substellar objects detected were either clearly brown dwarfs (very massive, not in a close orbit around a main-sequence star) or clearly planets (lower mass, orbiting close to their stars). However, as the number of discoveries of substeller objects grew to the dozens and then hundreds, there increasingly appeared to be overlap in the apparent mass distributions of brown dwarfs and planets. This highlighted the need to clarify the taxonomy. Moreover, the various definitions have been strained by the recent discoveries of objects such as CoRoT-3b, a ∼22-Jupiter-mass (M_J) object in a close (0.057-AU) orbit around its star (Deleuil et al. 2008) and the directly imaged objects of masses ∼5-15 M_J at tens of AU from HR 8799 and Fomalhaut (Marois et al. 2008; Kalas et al. 2008).

A commonly used way to classify objects that are ∼10-15 times the mass of Jupiter is by whether they fuse deuterium (D) in their deep interiors. This criterion was adopted in 2002 by the Working Group on Extrasolar Planets of the International Astronomical Union (Boss et al. 2007):

> *1) Objects with true masses below the limiting mass for thermonuclear fusion of deuterium (currently calculated to be 13 Jupiter masses for objects of solar metallicity) that orbit stars or stellar remnants are "planets" (no matter how they formed). The minimum mass/size required for an extrasolar object to be considered a planet should be the same as that used in our Solar System.*
> *2) Substellar objects with true masses above the limiting mass for thermonuclear fusion of deuterium are "brown dwarfs," no matter how they formed nor where they are located.*
> *3) Free-floating objects in young star clusters with masses below the limiting mass for thermonuclear fusion of deuterium are not "planets," but are "sub-brown dwarfs" (or whatever name is most appropriate).*

Although we (and others) do not necessarily endorse the "deuterium-burning edge" as the most useful delineation between planets and brown dwarfs[1] (see Burrows et al. 2001, Chabrier et al. 2005, and Bakos et al. 2010), it is a commonly used criterion and warrants further exploration.

Models of brown dwarfs and giant planets have been calculated since before the first such objects were discovered (Kumar 1963; Zapolsky & Salpeter 1969; Grossman & Graboske 1973; Burrows et al. 1993; Saumon et al. 1994; Burrows et al. 1995). Such computations depended heavily on the equation of state (EOS), and were therefore aided by

[1] Indeed, note that the IAU did not adopt this criterion. See, e.g., http://astrobob.lagunacollege.edu/~basri/defineplanet/Mercury.htm.

dsp@astro.princeton.edu, burrows@astro.princeton.edu, milsom@physics.arizona.edu

the publication of a new EOS for H_2-He mixtures (Saumon et al. 1995). In addition, models of the emergent radiation from, and of the temporal evolution of, brown dwarfs were improved by the application of nongray radiative transfer theory (Burrows et al. 1997, 1998; Burrows & Sharp 1999; Burrows 1999; Burrows et al. 2001, 2003; Baraffe et al. 2002, 2003; Allard et al. 2003; Chabrier et al. 2000b,a; Chabrier & Baraffe 2000; Sharp & Burrows 2007; Barman 2008) and sophisticated chemical models (Fegley & Lodders 1994; Lodders & Fegley 2002; Burrows & Sharp 1999; Sharp & Burrows 2007; Allard & Hauschildt 1995).

The theoretical study of brown dwarfs and massive planets is now a maturing field that is of particular current interest, given the increasing pace of discovery of objects in this mass range. Previous model calculations have suggested that deuterium burning turns on near a mass of 13 M_J (Burrows et al. 1997, 2001) or at 0.012 $M_\odot$ ($\sim$12.5 M_J, Chabrier et al. 2005).[2] An early such calculation was performed by Grossman & Graboske (1973), who claimed the existence of a deuterium main sequence near $0.012 M_\odot$. However, their models used a deuterium fraction that was about 10 times the Galactic value, and the atmosphere treatment was less sophisticated than the current state-of-the-art. Although previous calculations, and community prejudices, have converged on a mass limit of $\sim$13 M_J, and this mass range does provide a reasonable estimate for the mass at which significant deuterium burning occurs, it is worthwhile to clarify the precise range of deuterium-burning-mass predictions under a variety of model assumptions.

In this paper, we consider various models and nuclear burning criteria. In §2, we describe the models under consideration. We vary the helium fraction as a proxy for the effect of varied concentrations of elements heavier than hydrogen (§2.1); we vary the initial fraction of deuterium (§2.2); and we vary the metallicity in the context of its influence on atmospheric opacity and cooling (§2.3). In §3, we describe the influence that each aforementioned knob has on deuterium-burning, and in §4, we calculate derivatives of the D-burning mass edge with respect to each quantity (Y, $y_{\rm D,i}$, Z). In §5, we conclude by discussing the implications of our results for the distinction between brown dwarfs and giant planets.

2. MODELS

We consider brown dwarf/planet models of the sort described in Burrows et al. (2003). Specifically, objects are assumed to be born with significant interior entropy. In the deep interiors of such objects, conditions are ripe for non-negligible burning of deuterium through the reaction $p + D \rightarrow \gamma + {}^3{\rm He}$. The rate of deuterium burning depends on the concentration of deuterium, the mass-density, and a high power of temperature, going roughly as

$$\epsilon_{\rm D} \propto \rho y_{\rm D} T^{11.8}\,, \qquad (1)$$

for $T \sim 10^6$ K, where $\epsilon_{\rm D}$ is the specific deuterium-burning rate, ρ and T are central values of density and temperature, and y_D is the deuterium mixing ratio (Stahler 1988). The form of eq. (1) informs our choice of parameters to adjust in our models.[3] We vary the helium mass fraction (Y, which influences ρ_C), we vary the initial deuterium mixing fraction ($y_{\rm D,i}$), and we vary the metallicity of the atmosphere (Z, which strongly affects the opacity). Our models are summarized in Table 1 and described in §2.1-2.3 below. Note that each row of this table actually corresponds to a family of models with a dense spacing of masses, ranging from 10 to 20 times Jupiter's mass.

2.1. *Helium Fraction*

For an ideal gas, density depends on molecular weight, while for degenerate matter, density is inversely related to the ratio of electrons to baryons. The abundance of heavier-than-hydrogen elements affects the density for both reasons. We vary the helium content of our models from $Y = 0.22$ to $Y = 0.32$, with more helium-rich models representing objects that are richer in both helium and metals. The corresponding model names (in Table 1 and in the figures) are He22 – He32. Model He25 has helium mass-fraction 0.25, and is also referred to as model D2 (described in §2.2). These models have a radiative boundary condition (i.e. atmospheric opacities) calculated using the method of Burrows et al. (1997), with solar-metallicity opacities and initial deuterium number fraction of $y_{\rm D,i} = 2 \times 10^{-5}$.

2.2. *Initial Deuterium Fraction*

Big-bang nucleosynthesis calculations, in conjunction with other observations (CMB, high-z quasars, etc.) suggest that the primordial D:H ratio is $(2.8 \pm 0.2) \times 10^{-5}$ (Pettini et al. 2008). Our galaxy, however, is somewhat depleted in deuterium, relative to this value. Recent observations indicate that the mean mixing ratio of deuterium in the interstellar medium is roughly $(2.0 \pm 0.1) \times 10^{-5}$, though the scatter (among different lines of sight) is a factor of several (Prodanović et al. 2010). In our models, we take initial deuterium fractions of 10^{-5}, 2×10^{-5}, and 4×10^{-5} (mixing ratios).[4] The corresponding model

[2] Calculations such as this implicitly assume that objects start with large initial entropies (which leads, eventually, to high central temperatures), as is expected for bodies that form from the collapse of a cloud of molecular gas (Marley et al. 2007). Note that if the initial entropy is low, objects that are significantly more massive could, in principle, avoid burning any significant amount of deuterium, though formation scenarios such as this are probably not possible.

[3] Our actual deuterium-burning prescription is based on Fowler et al. (1975), but takes into account screening corrections (Saumon et al. 1996; Dewitt et al. 1996; Sahrling & Chabrier 1998).

[4] Values below this range are not rare (Prodanović et al. 2010).

names are D1, D2, and D4. These models also have a radiative boundary condition (i.e. atmospheric opacities) calculated using the method of Burrows et al. (1997), with solar-metallicity opacities and a helium mass-fraction of 0.25.

2.3. *Metallicity*

For a non-irradiated object, the metallicity, i.e. the abundance of elements heavier than helium, is the main determinant of the atmospheric chemistry and, hence, the opacity. Among objects with thick H_2-He-dominated atmospheres, this abundance can range from very low, to more than 30 times the solar abundance, as is expected for objects such as Uranus, Neptune, and similar-mass exoplanets (Guillot & Gautier 2007; Spiegel et al. 2010; Lewis et al. 2010; Nettelmann et al. 2010; Madhusudhan & Seager 2010). Still, objects as massive 10 M_J might generally be expected to have metallicities not much more than 0.5–1 dex more than solar. In our models, we take metallicity values ranging from zero up to a half dex more than solar, and we calculate the opacity corresponding to equilibrium chemistry (Burrows & Sharp 1999). In the zero-metallicity models, atmospheric opacity results entirely from collisionally-induced absorption due to the collisionally-induced dipoles of H_2 and He (Borysow et al. 1989). Though the bottom end of this range (0 and 0.01 times solar) includes lower metallicities than might be expected in most brown dwarfs, it is interesting to consider the full range of possibilities. These models fall into two sequences, Z0.01, Z0.1, Z0.3, Z1.0, and T0.3, T1, T3. Models in the former sequence are calculated using the opacities of Allard & Hauschildt (1995) to derive the atmospheric boundary conditions (D. Saumon, private communication) that drive the evolution. These models have a helium mass-fraction of 0.25 and initial deuterium fraction of 2×10^{-5}. The metallicity of these models (as a fraction of solar) is the number following the Z in the model name. Those in the latter sequence have a boundary condition calculated using `COOLTLUSTLY` (Hubeny 1988; Hubeny & Lanz 1995; Hubeny et al. 2003; Burrows et al. 2006; Sharp & Burrows 2007), with the same helium and initial deuterium fractions (Heng & Burrows 2010 in prep.). Among these, the metallicities of T0.3 and T3 are not exactly 0.3 and 3, but instead $10^{-1/2}$ and $10^{1/2}$ times solar metallicity. Finally, model Z0 has zero metallicity and is grouped by label with the former sequence, but actually has a radiative boundary condition taken from Saumon et al. (1994).

3. RESULTS

By considering a range of model parameters (Y, $y_{\rm D,i}$, Z) and atmospheric radiative boundary conditions, and by examining evolutionary trajectories for a range of masses, at ages from 1 Myr to 10 Gyr, we have produced a broad range of model calculations. Here, we show how properties such as radius, effective temperature, and the deuterium burning rate and power vary with time as a function of mass (§3.1). Furthermore, we examine how these evolutionary tracks vary with the other parameters at fixed mass (§3.2), and we calculate the variation of the deuterium-burning mass limit with the model parameters listed above (§3.3).

3.1. *Evolution with Mass*

The basic character of brown dwarf cooling trajectories is well known from a number of calculations in the last several decades, but it is worthwhile to examine the specific behavior of our models. We begin with an illustrative set of evolutionary trajectories for a representative family of models (He25, or D2). Figure 1 shows the evolution of four quantities that our models track.

The top panels show quantities related to model cooling. The top left panel shows the evolution of radius with time, and the top right panel shows the evolution of effective temperature with time. It is instructive to examine these two panels together. Higher mass objects begin larger but have higher effective temperatures and therefore cool more rapidly. As a result of their faster cooling, the radii of more massive objects shrink more rapidly, eventually (after roughly a gigayear) overtaking lower mass objects in radius. By the end of the calculation (after 10 Gyr), all objects are very nearly Jupiter's radius, but more massive objects are slightly smaller.

The lower panels of Fig. 1 are related to the fusion of deuterium. During the initial Hayashi-track stages of evolution, the luminosity is dominated by Kelvin-Helmholtz contraction. After a few million years, the central part of the object reaches temperatures and densities at which the deuterium fusion rate is non-negligible. The bottom left panel shows the ratio of the power from nuclear (deuterium) burning to the total luminosity. For the most massive objects, this ratio reaches fairly large values (well over 80%). However, the main sequence is where this ratio is essentially 100% (i.e., where Kelvin-Helmholtz contraction has ceased), and so it is clear that none of these models goes through a deuterium main sequence stage. The bottom right panel shows the evolution of the fraction of the initial deuterium (in this case, $y_{\rm D,i} = 2 \times 10^{-5}$) that has burned. Higher mass objects burn a larger fraction of their initial deuterium, and do so faster than lower mass objects. Regardless of mass, very little deuterium burns after a few hundred million years. Note, in comparing the top row to the bottom row, that the 15-M_J and 20-M_J models, which fuse the greatest amount of deuterium (among the models displayed), cool and shrink very quickly after the deuterium-burning phase.

3.2. *Model-Dependence of D-Burning Evolution*

In Fig. 2, we examine the deuterium-burning evolutionary profiles of 13-M_J objects from a variety of models. Each row shows analogous plots to the bottom row of Fig. 1, only instead of different curves representing different mass objects, they represent different model properties. The left column shows the evolution of the ratio of nuclear power to total luminosity, and the right column shows the fraction of the initial deuterium that burns. The three rows show, from top to bottom, models He22–He32 (varying helium fraction), models D1–D4 (varying initial deuterium fraction), and models Z0–Z1.0 (varying metallicity through its influence on atmospheric opacity). Each row also shows models He25 (which is also D2) and Z1.0, for comparison to "fiducial" models.

First, it is important to note the difference *at fixed model parameters* of the radiative boundary condition. The Z-sequence models have higher opacity, which leads to slower cooling, than the other models (which have the Burrows et al. 1997 boundary condition). As a result, models Z1.0 and He25/D2, which are otherwise identical, have markedly different evolutionary trajectories. The former reaches a peak nuclear-to-total power ratio of ≈80%, while the latter reaches only ≈50%. Furthermore, the former eventually burns 66% of its initial deuterium, while the latter burns only 17% of its. In fact, of the Z-sequence models, model Z0.3 (with 0.316× solar elemental abundance) more nearly approximates the He25/D2 evolution than does Z1.0. With its slower cooling, model Z1.0 has a moderate nuclear-burning to total luminosity ratio until later times; the ratio shown in the left column stays above 5% until ∼5 Gyr.

More generally, within each row of Fig. 2, the expected trends hold. The top row shows that more helium-rich models burn a greater fraction of their initial deuterium, which is unsurprising because these are the models with fewer electrons to support the mass via degeneracy pressure; thus, these models have denser, hotter cores. The middle row shows that models with higher initial deuterium content burn a greater fraction of their initial deuterium. This is a somewhat subtle point, because the y_D-term in eq. (1) would suggest that, other things being equal, the fractional depletion of deuterium with time should be constant irrespective of initial deuterium abundance. However, other things are not equal. In particular, the central temperature of more deuterium-rich models is maintained at a higher value for a longer period of time. As a result, the integrated fractional amount of deuterium burned is greater for these models. The bottom row shows that more metal-rich models burn a greater fraction of their initial deuterium, which stands to reason because their higher opacities produce a blanket effect, allowing them to maintain higher core temperatures for a longer time.

3.3. *Model-Dependence of D-Burning Limit*

We now quantify the deuterium-burning mass limit, and its dependence on the various model parameters we have varied. Figure 3 displays the same basic information in two different ways. In the left column, the fraction of the initial deuterium that combusts within 10 Gyr is plotted versus object mass. Horizontal dashed lines are plotted at 10%, 50%, and 90%, illustrating various (arbitrary) deuterium-burning cut-offs. The right column plots the deuterium-burning mass edge for each of these three criteria (i.e., the mass at the intersection of each curve in the left column with the corresponding dashed line) as a function of the three tunable model parameters: Y, $y_{\rm D,i}$, and Z. From top to bottom, the rows show the same respective model sets as in Fig. 2. As in Fig. 2, models He25/D2 and Z1.0 are shown in all three panels of the left column. The last three columns of Table 1 contain the same information as the right column of Fig. 3, and also include data for the `COOLTLUSTY` sequence of models (T0.3–T3). Note that the solar-metallicity `COOLTLUSTY` model (T1) and the fiducial Burrows et al. (1997) model (He25/D2) are quite similar to one another.

There are four main lessons from the data in Fig. 3 and Table 1:

1. Within each sequence of models, the expected trends hold. That is, greater helium abundance, greater deuterium abundance, and higher metallicity allow a given amount of deuterium to fuse at a lower object mass.

2. Depending on what is meant by "deuterium burning" (i.e., how much of the initial deuterium must burn to qualify), the deuterium-burning mass limit can vary quite a bit. As the criterion goes from 10% to 50% and from 50% to 90%, the required mass increases by ∼0.8-0.9 M_J.

3. 0.012 $M_\odot$ and 13 M_J is not far from the mass limit for most models.

4. However, the full range of masses displayed in this table goes from 11.3 M_J (He32, 10%) to 16.3 M_J (Z0, 90%).

With the final point in mind, it is clear that claiming that an object does or does not "burn deuterium" implies a set of physical assumptions about the model and a criterion for deuterium burning. Any criterion is fine, so long as people know what it is; but implicit assumptions should be made explicit, and might not actually apply to some astrophysical objects.

4. DISCUSSION

A useful way to quantify the influence of varying the model parameters on the deuterium mass limit is with the derivative of the mass-limit with respect to each model parameter. Although the curves in the

right column of Fig. 3 do not have constant slope, they are not very far from linear over the ranges shown. In Table 2, we present the average derivative with respect to each parameter. For Y and $y_{\rm D,i}$, we take linear derivatives; for $y_{\rm D,i}$ and Z, we take logarithmic derivatives. These derivatives are not terribly precise measures of the variation, but allow for a quick, crude estimate of the deuterium edge-mass at different parameter values.

Note that, in the calculations discussed so far, the effect of higher metallicity has been reflected only in the atmospheric opacity. In a real object, however, higher metallicity throughout would also lead to an EOS change for the bulk, because high-Z elements have lower electron-to-baryon ratios. As a result, a higher metallicity object would have a higher central density than occurs in our models, and would therefore have a lower deuterium mass limit than we have shown, particularly for model T3. We can approximately correct for this by using a higher helium fraction. We, therefore, have post-processed our models in an attempt to incorporate this effect. Using values from Asplund et al. (2009), we take $Y = 0.2703$ and $Z = 0.0142$ to be the helium and heavy-element mass-fractions corresponding to protosolar abundance. Motivated by this, we add 0.0142 in Y for every unit in metallicity (i.e., $Y = 0.2703{+}0.0142$ for solar, $Y = 0.2703{+}2{\times}0.0142$ for $2\times$ solar, etc.).[5] We perform a cubic interpolation in Y and use the Z-derivative for model sequence T0.3–T3 to calculate the values in Table 3 corresponding to 0.5, 1, 2, and 3 times solar metallicity. Values of the edge mass in this table then range from $\sim$11.0 M_J ($3\times$ solar, 10% of initial deuterium burned) to $\sim$13.9 M_J ($0.5\times$ solar, 90% of initial deuterium burned).

Although the deuterium-burning mass limits in Tables 1 and 3 vary from 11.0 to 16.3 times Jupiter's mass, a narrower range of values is found if we restrict our attention to a particular burning fraction criterion (50%, say) with realistic Y, $y_{\rm D,i}$, and Z values. For helium mass-fractions between 0.25 and 0.30, initial deuterium fractions between 10^{-5} and 2×10^{-5}, and metallicities between 0.5 and 2 times solar, the mass required to burn 50% of the initial deuterium is between $\sim$12.2 M_J and $\sim$13.7 M_J. Values somewhat outside this range are not impossible, but values very far from this range are probably rare.

5. CONCLUSIONS

We have calculated a suite of models of substellar mass objects, encompassing a range of values of helium fraction, initial deuterium fraction, and metallicity. We have also used several calculations of the atmospheric boundary conditions. Although the rate of deuterium-burning is extremely sensitive to temperature, it is worthwhile bearing in mind that deuterium will burn at *some* rate at any nonzero temperature, so one must specify what is meant by "deuterium burning" (i.e., how much of the initial deuterium must burn to qualify). We have found that, depending on what criterion is used, reasonable values for the deuterium mass limit range from $\sim$11.4 to $\sim$14.4 times Jupiter's mass; the former limit corresponding to $2\times$ solar metallicity, 10% of initial deuterium burned, and the latter limit to solar metallicity, $Y = 0.25$, 90% of initial deuterium burned. Extreme models (very low helium fraction, very low metallicity) could require even higher mass in order to burn a specified percentage of their initial deuterium. The canonical value of 13 M_J (Burrows et al. 1997) is a reasonable estimate of the mass at which signifcant deuterium burning begins, but this value is model-dependent.

Still, one should keep in mind that the deuterium cut is probably less relevant to an object's true taxonomic status than is its formation history. The downside of a "formation scenario" definition is that formation history is not easily observable. On the other hand, though mass might be observable, the parameters Y, $y_{\rm D,i}$, and Z might not be. Furthermore, some objects will be found significantly above 13 M_J that will be of clearly "planetary" origin (e.g., CoRoT-3b). Whether to call these objects "brown dwarfs" or "deuterium-burning planets" remains open for debate. Similarly, objects might be found that are significantly less massive than 13 M_J that appear not to have formed in a protoplanetary disk, but rather to be the low-mass end of the brown dwarf formation process. Though classified as "planets" by standard terminology, these objects might be more taxonomically related to brown dwarfs than to planets.

We emphasize that there is really no need at this time to rigidly distinguish between a giant planet and a brown dwarf on the basis of a single criterion. There is ambiguity in the provenance of these objects, and this ambiguity might persist for a while. The use of a particular term ("planet" or "brown dwarf"), should be accompanied by the definition that is employed. Given that planets are thought to be objects in orbit around a star (or around a brown dwarf), while brown dwarfs are thought to be the low-mass end of the star formation process, there is likely to be overlap in the mass range of these objects unless one adopts a rigid mass cut to distinguish them. Doing so, however, will surely lead to an overlap in formation scenarios (as in the case of CoRoT-3b). When classifying a newly-discovered substellar-mass object, one can use a variety of "reasonable" criteria, but the classifications should remain tentative until a more thorough observational and theoretical understanding of substellar objects is achieved.

We thank Kevin Heng, Bill Hubbard, Didier Saumon, Jason Nordhaus, and Zimri Yaseen for use-

[5] It is not clear that the equivalent ΔY for solar metallicity should be exactly Z, but this seems a reasonable first approximation.

ful discussions. This study was supported in part by NASA grant NNX07AG80G. We also acknowledge support through JPL/Spitzer Agreements 1328092, 1348668, and 1312647.

REFERENCES

Allard, F. & Hauschildt, P. H. 1995, ApJ, 445, 433
Allard, N. F., Allard, F., Hauschildt, P. H., Kielkopf, J. F., & Machin, L. 2003, A&A, 411, L473
Asplund, M., Grevesse, N., Sauval, A. J., & Scott, P. 2009, ARA&A, 47, 481
Bakos, G. Á., Hartman, J., Torres, G., Latham, D. W., Kovács, G., Noyes, R. W., Fischer, D. A., Johnson, J. A., Marcy, G. W., Howard, A. W., Kipping, D., Esquerdo, G. A., Shporer, A., Béky, B., Buchhave, L. A., Perumpilly, G., Everett, M., Sasselov, D. D., Stefanik, R. P., Lázár, J., Papp, I., & Sári, P. 2010, ArXiv e-prints
Baraffe, I., Chabrier, G., Allard, F., & Hauschildt, P. H. 2002, A&A, 382, 563
Baraffe, I., Chabrier, G., Barman, T. S., Allard, F., & Hauschildt, P. H. 2003, A&A, 402, 701
Barman, T. S. 2008, in Astronomical Society of the Pacific Conference Series, Vol. 384, 14th Cambridge Workshop on Cool Stars, Stellar Systems, and the Sun, ed. G. van Belle, 133–+
Borysow, A., Frommhold, L., & Moraldi, M. 1989, ApJ, 336, 495
Boss, A. P., Butler, R. P., Hubbard, W. B., Ianna, P. A., Kürster, M., Lissauer, J. J., Mayor, M., Meech, K. J., Mignard, F., Penny, A. J., Quirrenbach, A., Tarter, J. C., & Vidal-Madjar, A. 2007, Transactions of the International Astronomical Union, Series A, 26, 183
Burrows, A. 1999, Science, 285, 847
Burrows, A., Hubbard, W. B., Lunine, J. I., & Liebert, J. 2001, Reviews of Modern Physics, 73, 719
Burrows, A., Hubbard, W. B., Lunine, J. I., Marley, M., & Saumon, D. 1998, ArXiv Astrophysics e-prints
Burrows, A., Hubbard, W. B., Saumon, D., & Lunine, J. I. 1993, ApJ, 406, 158
Burrows, A., Marley, M., Hubbard, W. B., Lunine, J. I., Guillot, T., Saumon, D., Freedman, R., Sudarsky, D., & Sharp, C. 1997, ApJ, 491, 856
Burrows, A., Saumon, D., Guillot, T., Hubbard, W. B., & Lunine, J. I. 1995, Nature, 375, 299
Burrows, A. & Sharp, C. M. 1999, ApJ, 512, 843
Burrows, A., Sudarsky, D., & Hubeny, I. 2006, ApJ, 650, 1140
Burrows, A., Sudarsky, D., & Lunine, J. I. 2003, ApJ, 596, 587
Chabrier, G. & Baraffe, I. 2000, ARA&A, 38, 337
Chabrier, G., Baraffe, I., Allard, F., & Hauschildt, P. 2000a, ApJ, 542, L119
—. 2000b, ApJ, 542, 464
Chabrier, G., Baraffe, I., Allard, F., & Hauschildt, P. H. 2005, ArXiv Astrophysics e-prints
Deleuil, M., Deeg, H. J., Alonso, R., Bouchy, F., Rouan, D., Auvergne, M., Baglin, A., Aigrain, S., Almenara, J. M., Barbieri, M., Barge, P., Bruntt, H., Bordé, P., Collier Cameron, A., Csizmadia, S., de La Reza, R., Dvorak, R., Erikson, A., Fridlund, M., Gandolfi, D., Gillon, M., Guenther, E., Guillot, T., Hatzes, A., Hébrard, G., Jorda, L., Lammer, H., Léger, A., Llebaria, A., Loeillet, B., Mayor, M., Mazeh, T., Moutou, C., Ollivier, M., Pätzold, M., Pont, F., Queloz, D., Rauer, H., Schneider, J., Shporer, A., Wuchterl, G., & Zucker, S. 2008, A&A, 491, 889
Dewitt, H., Slattery, W., & Chabrier, G. 1996, Physica B Condensed Matter, 228, 21
Fegley, B. J. & Lodders, K. 1994, Icarus, 110, 117
Fowler, W. A., Caughlan, G. R., & Zimmerman, B. A. 1975, ARA&A, 13, 69
Grossman, A. S. & Graboske, H. C. 1973, ApJ, 180, 195
Guillot, T. & Gautier, D. 2007, Treatise on Geophysics, Planets and Moons, vol. 10 (Elsevier, Amsterdam)
Heng, K. & Burrows, A. 2010 in prep., ApJ
Hubeny, I. 1988, Computer Physics Communications, 52, 103
Hubeny, I., Burrows, A., & Sudarsky, D. 2003, ApJ, 594, 1011
Hubeny, I. & Lanz, T. 1995, ApJ, 439, 875
Kalas, P., Graham, J. R., Chiang, E., Fitzgerald, M. P., Clampin, M., Kite, E. S., Stapelfeldt, K., Marois, C., & Krist, J. 2008, Science, 322, 1345
Kumar, S. S. 1963, ApJ, 137, 1121
Lewis, N. K., Showman, A. P., Fortney, J. J., Marley, M. S., Freedman, R. S., & Lodders, K. 2010, ApJ, 720, 344
Lodders, K. & Fegley, B. 2002, Icarus, 155, 393
Madhusudhan, N. & Seager, S. 2010, ArXiv e-prints
Marcy, G. W. & Butler, R. P. 1996, ApJ, 464, L147+
Marley, M. S., Fortney, J. J., Hubickyj, O., Bodenheimer, P., & Lissauer, J. J. 2007, ApJ, 655, 541
Marois, C., Macintosh, B., Barman, T., Zuckerman, B., Song, I., Patience, J., Lafrenière, D., & Doyon, R. 2008, Science, 322, 1348
Mayor, M. & Queloz, D. 1995, Nature, 378, 355
Nettelmann, N., Kramm, U., Redmer, R., & Neuhaeuser, R. 2010, ArXiv e-prints
Oppenheimer, B. R., Kulkarni, S. R., Matthews, K., & Nakajima, T. 1995, Science, 270, 1478
Pettini, M., Zych, B. J., Murphy, M. T., Lewis, A., & Steidel, C. C. 2008, MNRAS, 391, 1499
Prodanović, T., Steigman, G., & Fields, B. D. 2010, MNRAS, 406, 1108
Sahrling, M. & Chabrier, G. 1998, ApJ, 493, 879
Saumon, D., Bergeron, P., Lunine, J. I., Hubbard, W. B., & Burrows, A. 1994, ApJ, 424, 333
Saumon, D., Chabrier, G., & van Horn, H. M. 1995, ApJS, 99, 713
Saumon, D., Hubbard, W. B., Burrows, A., Guillot, T., Lunine, J. I., & Chabrier, G. 1996, ApJ, 460, 993
Sharp, C. M. & Burrows, A. 2007, ApJS, 168, 140
Spiegel, D. S., Burrows, A., Ibgui, L., Hubeny, I., & Milsom, J. A. 2010, ApJ, 709, 149
Stahler, S. W. 1988, ApJ, 332, 804
Zapolsky, H. S. & Salpeter, E. E. 1969, ApJ, 158, 809

TABLE 1
MODELS

Model	Z ($Z_\odot$)	$y_{\rm D,i}$	Y	M (10%) (M_J)	M (50%) (M_J)	M (90%) (M_J)
He22	1	2×10^{-5}	0.22	13.20	14.08	14.92
He25 (D2)[a]	1	2×10^{-5}	0.25	12.70	13.55	14.35
He28	1	2×10^{-5}	0.28	12.06	12.83	13.62
He30	1	2×10^{-5}	0.30	11.62	12.42	13.20
He32	1	2×10^{-5}	0.32	11.32	12.05	12.78
D1	1	1×10^{-5}	0.25	12.71	13.74	14.55
D2 (He25)	1	2×10^{-5}	0.25	12.70	13.55	14.35
D4	1	4×10^{-5}	0.25	12.45	13.09	13.93
Z0	0	2×10^{-5}	0.22	14.37	15.40	16.30
Z0.01	0.01	2×10^{-5}	0.22	13.59	14.56	15.39
Z0.1	0.1	2×10^{-5}	0.22	12.92	13.82	14.65
Z0.3	0.3	2×10^{-5}	0.22	12.48	13.33	14.14
Z1.0[b]	1	2×10^{-5}	0.22	12.00	12.79	13.56
T0.3	$10^{-1/2}$	1×10^{-5}	0.25	12.92	13.77	14.67
T1	1	2×10^{-5}	0.25	12.54	13.48	14.33
T3	$10^{1/2}$	4×10^{-5}	0.25	12.20	13.13	13.86

Models He22–He32 and D1–D4 are calculated with a Burrows et al. (1997) radiative boundary condition Models Z0.01–Z1.0 are calculated with opacities from Allard & Hauschildt (1995), incorporated in atmospheric boundary conditions as described in Burrows et al. (2001) (D. Saumon, private communication). Models T0.3–T3 have radiative boundary conditions calculated with `COOLTLUSTY`. Model Z0's radiative boundary condition comes from Saumon et al. (1994).

[a] This model shows up in two rows, named both He25 and D2, and is one of two "fiducial" models.

[b] This is the other "fiducial" model.

TABLE 2
Approximate Edge-Mass Derivatives

Model Sequence	Derivative	Derivative Value
He22–He32	$(dM/dY)/100$	$-0.2M_J$
D1–D4	$(dM/dy_{\rm D,i})/10^5$	$-0.16M_J$
D1–D4	$dM/d\log_{10}[y_{\rm D,i}]$	$-0.8M_J$
Z0.01–Z1.0	$dM/d\log_{10}[Z]$	$-0.9M_J$
T0.3–T3	$dM/d\log_{10}[Z]$	$-0.7M_J$

TABLE 3
Edge-Masses for "Realistic" Treatment of Z

Metallicity	M (10%) (M_J)	M (50%) (M_J)	M (90%) (M_J)
0.5× solar	12.26	13.10	13.93
1 × solar	11.89	12.73	13.57
2 × solar	11.39	12.23	13.06
3 × solar	10.99	11.83	12.67

We start with $Y = 0.2703$ and add 0.0142 in Y for every unit in Z. We perform a cubic interpolation in Y and use the derivatives recorded in the T0.3–T3 rows of Table 2 to approximate the combined affects of metallicity on pressure support and on atmospheric opacity.

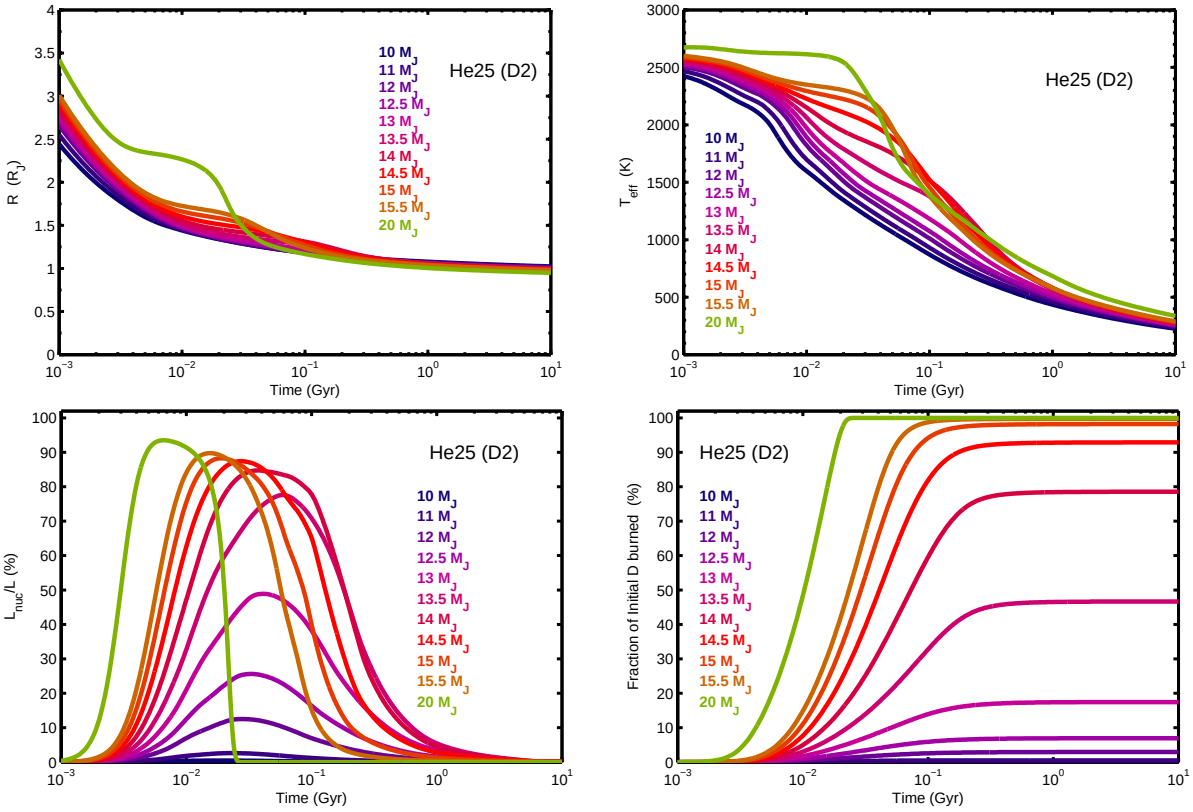

FIG. 1.— Evolutionary trajectories as functions of mass for D2 models. *Top left:* Radius vs. time. Higher mass objects cool faster and have smaller radii by 10 Gyr, even though they begin with larger radii. The 15-M_J and 20-M_J models cool and shrink particularly rapidly after the conclusion of deuterium burning. *Top Right:* Effective temperature vs. time. *Bottom left:* Ratio of nuclear power to total luminosity vs. time. *Bottom right:* Fraction of initial deuterium burned vs. time.

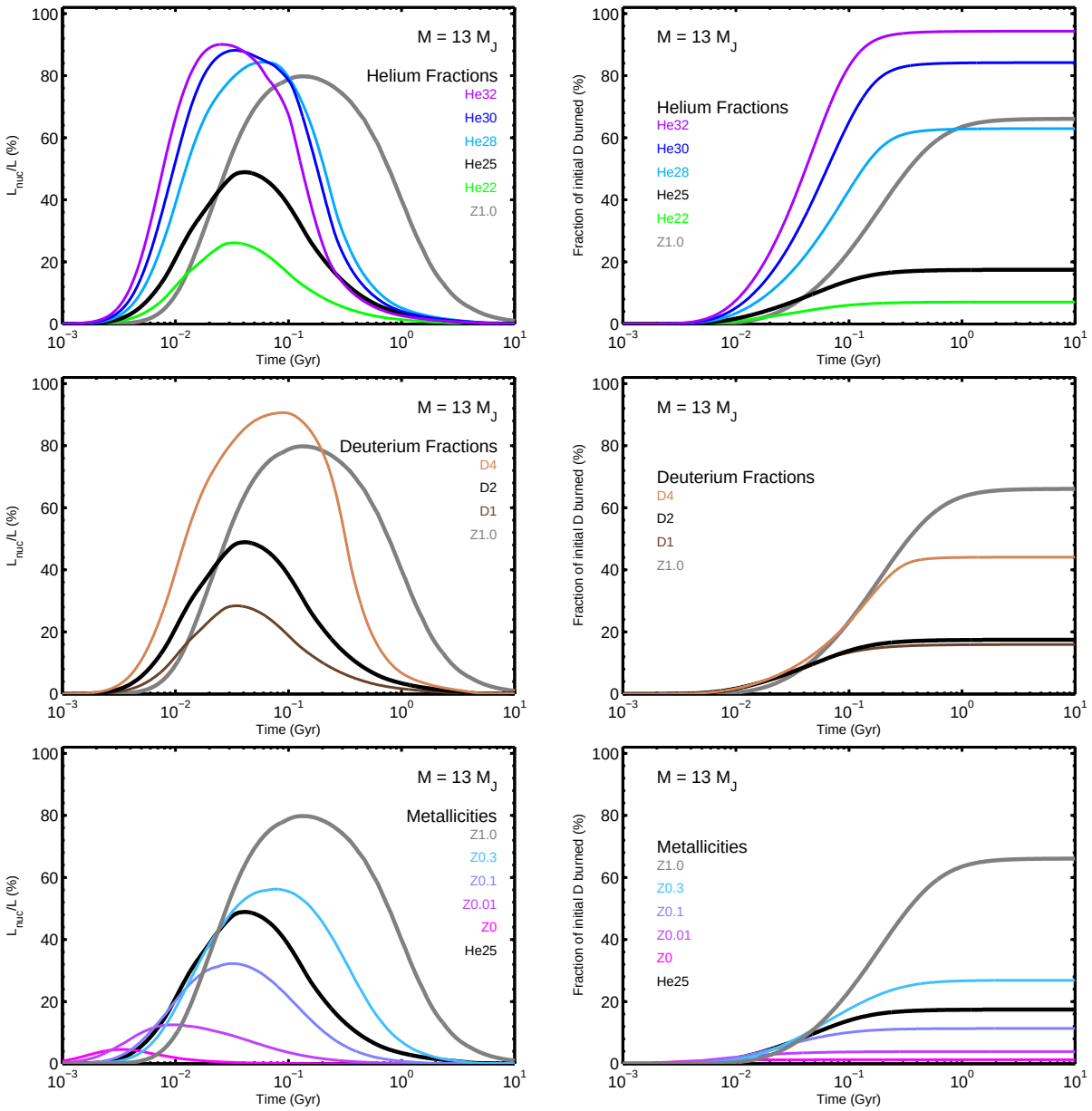

FIG. 2.— Ratio of nuclear power to total luminosity vs. time (*left*) and fraction of initial deuterium that burns vs. time (*right*), for 13-M_J models. Note that very little deuterium burning occurs after ∼1 Gyr. Models are grouped by varying the helium fraction (*top*), the initial deuterium fraction (*middle*), and the metallicity (*bottom*).

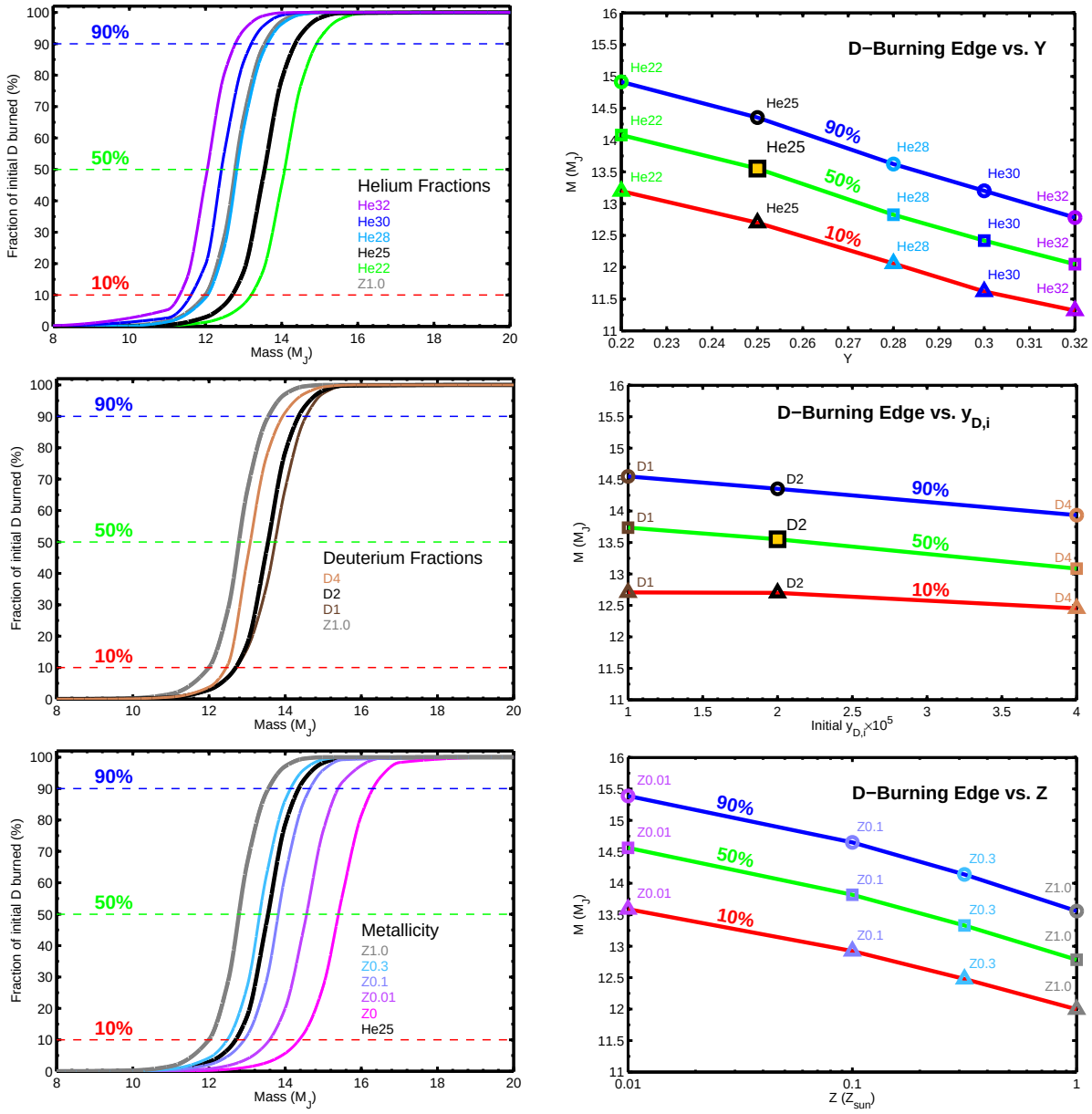

FIG. 3.— Fraction of initial deuterium that burns within 10 Gyr vs. Mass (*left*); and dependence of deuterium-burning edge on Y, $y_{D,i}$, and Z, for different "edge-criteria" (*right*).
Left: For a variety of models, the total fraction of the initial deuterium abundance that combusts through nuclear fusion within 10 Gyr is shown as a function of the object's mass. Note, per Fig. 2, that if any appreciable fraction of the initial deuterium ends up burning, this happens within the first 1 Gyr. Models He25/D2 and Z1.0 are shown in all three panels. In each panel, horizontal dashed lines are plotted at 10%, 50%, and 90%.
Top: For solar metallicity and initial deuterium number fraction of 2×10^{-5}, models from Burrows et al. (1997) are shown for different helium mass-fractions. Greater helium fraction leads to deuterium burning at a lower mass.
Middle: For solar metallicity and helium abundance (by mass) of 0.25, models from Burrows et al. (1997) are shown for different initial deuterium abundances. Greater initial deuterium abundance leads to deuterium burning at lower mass.
Bottom: For inital deuterium abundance of 2×10^{-5} and helium abundance of 0.25, models using an Allard & Hauschildt (1995) boundary condition (Z0.01, Z0.1, Z0.3, Z1.0) are shown. A model with zero metallicity (Z0, Saumon et al. 1994) is also shown. Greater metallicity leads to deuterium burning at lower mass.
Right: In each panel, the red, green, and blue curves correspond to edge-criteria of 10%, 50%, and 90% of the initial deuterium burning within 10 Gyr. These correspond to the masses at which the fraction-burned curves in the left panel of this figure cross the three horizontal dashed lines. Individual models are coded by the same colors as in the left panel. The mass of the deuterium burning edge is shown as a function of helium fraction (*top*), initial deuterium fraction (*middle*), and metallicity (*bottom*). The "fiducial model" He25/D2 is represented (in the top two panels) with a large black square, filled with yellow.